

Superconducting Phase with Fractional Vortices in the Frustrated Kagome Wire Network at $f = 1/2$

Kyungwha Park and David A. Huse

Department of Physics, Princeton University, Princeton, NJ 08544

November 3, 2018

Abstract

In classical XY kagome antiferromagnets, there can be a novel low temperature phase where $\psi^3 = e^{i3\theta}$ has quasi-long-range order but ψ is disordered, as well as more conventional antiferromagnetic phases where ψ is ordered in various possible patterns (θ is the angle of orientation of the spin). To investigate when these phases exist in a physical system, we study superconducting kagome wire networks in a transverse magnetic field when the magnetic flux through an elementary triangle is a half of a flux quantum. Within Ginzburg-Landau theory, we calculate the helicity moduli of each phase to estimate the Kosterlitz-Thouless (KT) transition temperatures. Then at the KT temperatures, we estimate the barriers to move vortices and effects that lift the large degeneracy in the possible ψ patterns. The effects we have considered are inductive couplings, non-zero wire width, and the order-by-disorder effect due to thermal fluctuations. The first two effects prefer $q = 0$ patterns while the last one selects a $\sqrt{3} \times \sqrt{3}$ pattern of supercurrents. Using the parameters of recent experiments, we conclude that at the KT temperature, the non-zero wire width effect dominates, which stabilizes a conventional superconducting phase with a $q = 0$ current pattern. However, by adjusting the experimental parameters, for example by bending the wires a little, it appears that the novel ψ^3 superconducting phase can instead be stabilized. The barriers to vortex motion are low enough that the system can equilibrate into this phase.

1 Introduction

Consider the classical XY antiferromagnet on the kagome lattice, with Hamiltonian

$$\mathcal{H} = -J \sum_{\langle ij \rangle} \cos(\theta_i - \theta_j) , \quad (1)$$

where $J < 0$, the sum runs over all nearest neighbor pairs of sites, and θ_i is the orientation of the spin at site i . Because of the antiferromagnetic interactions, each elementary triangular plaquette is frustrated. The ground states of this system all have the angle $|\theta_i - \theta_j| = 2\pi/3$ between all pairs of nearest-neighbor spins. This results in just three different spin orientations, which we may call $\theta = 0, \pm 2\pi/3$, being present in the entire lattice. All three spin orientations are present on every elementary triangle of the lattice. Some examples of ground states are shown in Fig. 1. There are two types of simply periodic ground states that we will be particularly looking at. One type is ordered with zero crystal momentum, meaning the spin pattern has the same translational symmetries as the lattice. This type of ground state is called “ $q = 0$ ” [1] and is shown in Fig. 1 (a). The other simple ground state is called “ $\sqrt{3} \times \sqrt{3}$ ” (Fig. 1 (b)). This pattern has a unit cell which consists of three hexagons and which has a linear dimension $\sqrt{3}$ times larger than the grid’s unit cell, thus its name [1]. Unlike these simple patterns, almost all ground states are instead irregular and nonperiodic. We call them “random” patterns. One of these random patterns is shown in Fig. 1 (c). Because of the massive discrete degeneracy of the ground state patterns of $\psi = e^{i\theta}$, this system has an extensive ground-state entropy of roughly $0.126k_B$ per site [2], in addition to the usual continuous rotational degeneracy of the XY spins. This frustration-induced extensive degeneracy leads to a novel low-temperature ordered phase [3][4]. In the novel low temperature phase, $\psi^3 = e^{i3\theta}$ has quasi-long range order but the usual order parameter ψ has only short-range correlations. Since the model is a two-dimensional XY model, the low temperature phase appears only below a Kosterlitz-Thouless (KT) transition temperature. [5] The vortices that unbind at this KT transition are vortices of ψ^3 , and thus fractional $1/3$ -vortices in ψ .

Physical systems that realize frustrated XY models are superconducting Josephson junctions or wire networks on the kagome lattice in a transverse magnetic field. In these systems the different spin patterns of the magnetic model are realized as patterns of supercurrents. In the kagome-lattice antiferromagnet the elementary triangular plaquettes are maximally frustrated, which occurs for the kagome superconducting Josephson junctions or wire networks when the magnetic flux through each elementary triangular plaquette is one-half of a flux quantum (or any odd multiple thereof). For a uniform field that maximally frustrates the triangular plaquettes, the resulting flux through the hexagonal plaquettes of the kagome lattice is an integer number of flux quanta, which means these plaquettes are not frustrated, just as in the XY antiferromagnet. The novel phase of interest does not have conventional superconductivity, with quasi-long-range order (QLRO) in the phase θ of the Cooper pairs, but does have QLRO in the phase 3θ of “Cooper sextuples”. It is in this sense a rather exotic form of superconductivity.

Recently, an exciting experimental result [6][7] has emerged from aluminum kagome wire networks when the applied magnetic flux per triangular plaquette is one half of a flux quantum. The result is that an ordered phase is appearing at this magnetic field, in contrast to the mean field prediction [8]. Motivated by these experimental data, in this paper we study this novel ψ^3 phase and other more conventional ordered phases in

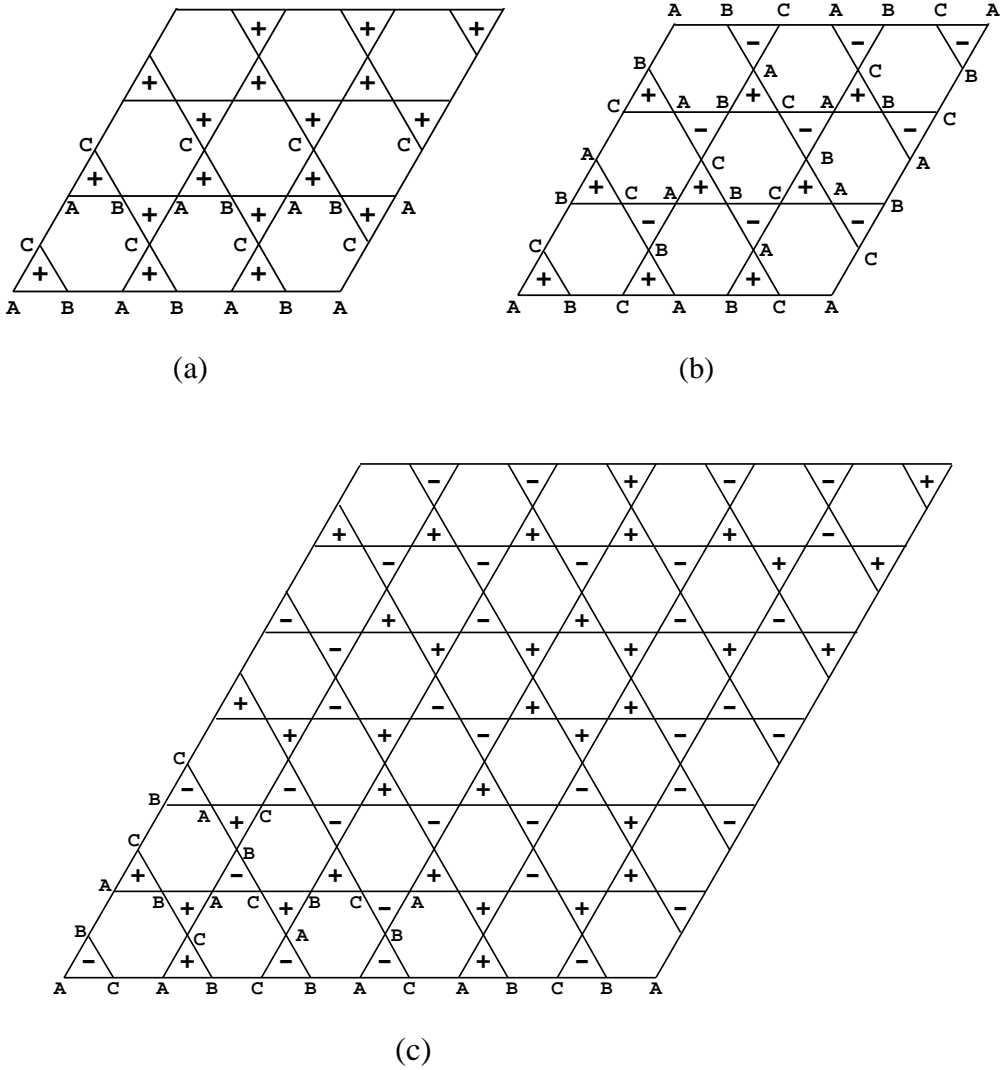


Figure 1: Some ground state patterns of the classical XY kagome antiferromagnet. Periodic boundary conditions are applied to these finite lattices. A , B , and C are the three possible spin orientations at each site, $\theta = 0, \pm 2\pi/3$. When, on moving counterclockwise around a triangle, the spins rotate counterclockwise (clockwise) in spin space, a + (-) sign is assigned to the triangle. (a) One of the two $q = 0$ patterns. (b) One of the two $\sqrt{3} \times \sqrt{3}$ patterns. (c) One of the random patterns.

kagome superconducting wire networks. However, the superconducting wire network does not *precisely* realize the model (1), because (i) the material and connections do not consist of perfect mathematical points and straight lines, (ii) there are also long-range inductive interactions between the supercurrents, and (iii) both the *magnitude* and the phase of the superconducting order parameter can vary near the temperatures of interest. All these (and possibly other) effects lift the precise degeneracy that underlies the novel ψ^3 phase, meaning the question of whether or not it can actually be realized experimentally requires some more investigation. This is the topic of this paper. We conclude that for the parameters of the recent experiments (as summarized in Appendix A) the novel ψ^3 ordered phase does not occur; instead the system orders into a $q = 0$ supercurrent pattern with conventional superconducting order. But the novel ψ^3 phase can be stabilized if one adjusts some experimental parameters such as by bending the wires a little or making the wires narrower.

2 Model and its Possible Superconducting Phases

We model the superconducting wire array with the usual Ginzburg-Landau (GL) free energy functional:

$$F = \int d^3x [\alpha |\psi|^2 + \frac{\beta |\psi|^4}{2} + \frac{1}{2m^*} |(\frac{\hbar}{i} \vec{\nabla} - \frac{e^*}{c} \vec{A}) \psi|^2] , \quad (2)$$

where the integral runs over the volume occupied by the wires. The wires form a kagome grid, with distance a between junctions. The wire pattern is invariant under translations by $2a$ parallel to any wire, and also has all the point group symmetries of the ideal kagome lattice. At first we will assume the wires are straight and quite thin, with a rectangular cross-section of in-plane width w and thickness d . [Later we will explicitly consider effects due to the nonzero width of the wires and due to possibly bending the wires away from straight.] In this thin-wire limit, any variation of the order parameter or vector potential across the wires is neglected, so the model treats the wires as ideal lines and the junctions as points. At this point we also neglect the energy of the magnetic fields produced by the supercurrents. These inductive effects are estimated below and are negligible near the phase transition for the experimental parameters we will consider here. In zero magnetic field, the mean field phase transition temperature, T_c^m , is the temperature where $\alpha = 0$. We will be working below but generally quite near this temperature so will assume, as usual, that α varies linearly with the temperature T . We will neglect any temperature dependence of the other parameters in the free energy.

For convenience, we will use a , the distance between wire junctions, as our unit of length. In zero field the free energy is minimized when the magnitude of the order parameter $|\psi|$ is $\sqrt{\frac{|\alpha|}{\beta}}$ and we will use this as the unit for the order parameter. We use $\frac{\Phi_0}{2\pi a}$ as the unit of vector potential, where Φ_0 is the flux quantum (in our units, $\Phi_0 = 2\pi$). In these units the counter-clockwise integral of a vector potential \vec{A} of the external magnetic field around an

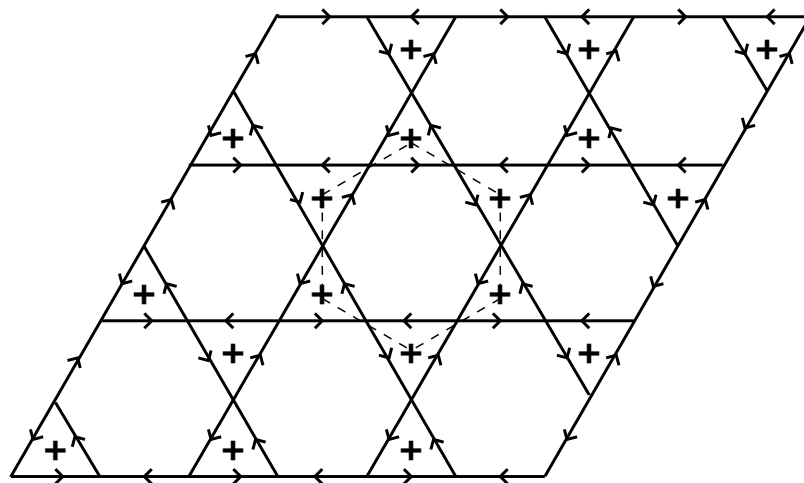
elementary triangular plaquette of the grid is $2\pi f$, where f is the applied magnetic flux passing through the triangle in units of the flux quantum. Finally, we use $\frac{H_c^2}{4\pi} = \frac{\alpha^2}{\beta}$ as our unit of free energy density. Note that our units of order parameter and free energy density are temperature-dependent. In these units and in the thin-wire limit without thermal fluctuations, the GL free energy is simply

$$F = wd \int ds [-|\psi|^2 + \frac{|\psi|^4}{2} + \xi_0^2 |(\nabla - iA)\psi|^2], \quad (3)$$

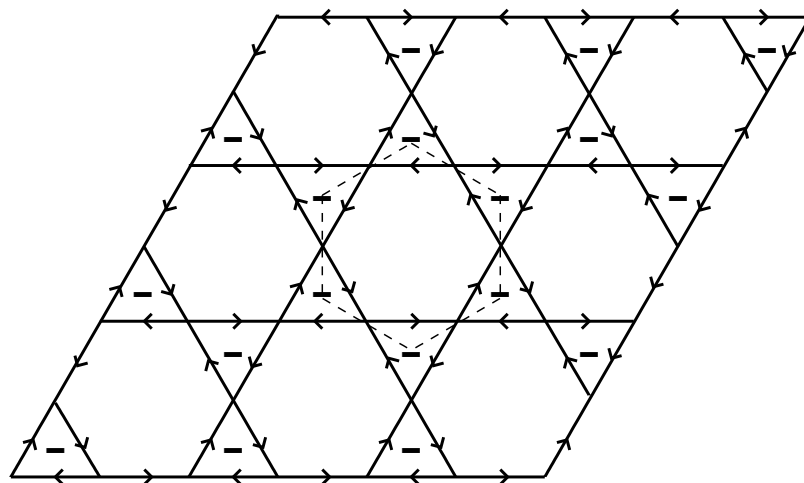
where now the integral, the vector potential, and the gradient are one-dimensional, running along all wires, and $\xi_0 = \frac{\hbar}{a\sqrt{2m^*|\alpha|}}$ is the mean-field coherence length in zero magnetic field, in units of the lattice spacing a . We define the amplitude for the divergence of this zero-field coherence length at T_c^m via $\xi_0(t) \approx \tilde{\xi}_0(1-t)^{-1/2}$, where $t = T/T_c^m$.

What order parameter patterns minimize our free energy (3) for the case of interest $f = 1/2$? Let us separate the order parameter into its magnitude and phase: $\psi = |\psi|e^{i\phi}$. The quantities that are gauge-invariant and thus physical are $|\psi|$ and the gauge-invariant phase gradient $\nabla_g\phi = (\nabla\phi - A)$, which is proportional to the velocity of the supercurrent. Because ψ is single-valued, the counter-clockwise integral of $\nabla_g\phi$ around any elementary triangle must be $2\pi(n-f)$ with n an integer. For $f = 1/2$, the free energy of a given triangle is minimized when $n - f = \pm 1/2$. These two degenerate states consist of supercurrents flowing either clockwise ($-$) or counterclockwise ($+$) around the triangle. In the lowest free energy states both $|\psi|$ and $\nabla_g\phi$ are uniform around the triangle, taking on the values $\nabla_g\phi_0 = \pm\pi/3$ and $|\psi_0|^2 = 1 - (\xi_0\pi/3a)^2$, provided the temperature is low enough that $\xi_0 \leq 3a/\pi$. For higher temperatures close to T_c^m where $\xi_0 > 3a/\pi$ the system is in the normal state for $f = 1/2$. The mean-field transition temperature $T_c^m(f)$ is minimized at $f = 1/2$ where the frustration is maximal,[8] with $1 - (T_c^m(f = 1/2)/T_c^m) \approx (\tilde{\xi}_0\pi/3a)^2$ for small $\tilde{\xi}_0/a$. We consider the case of small $\tilde{\xi}_0/a$, as in the recent experiments[7]. Then the suppression of the transition by the frustration is small, so Ginzburg-Landau theory remains a good approximation at $T_c^m(f = 1/2)$. To form an allowed current pattern of the entire grid out of these local ground states of the individual triangles one must also obey the constraint that ψ remains single-valued on passing around each elementary hexagonal plaquette. The area of a hexagon is six times that of a triangle so $6f$ flux quanta pass through each hexagon. For $f = 1/2$ this means the hexagons are not frustrated and the total gauge-invariant phase change around a hexagon must be an integer multiple of 2π . In the ground states of the triangles the gauge-invariant phase change along each wire segment is $\pm\pi/3$. Thus in an allowed minimum free energy state each hexagon either (a) has all the currents on its six edges going in the same direction (clockwise or counterclockwise) so the total change is $\pm 2\pi$ or (b) it has three edges with clockwise-going currents and three with counter-clockwise-going currents so the total vanishes. The entropy of such allowed states is roughly $0.4k_B$ per hexagonal unit cell.[2]

Some examples of current patterns that minimize our free energy (3) are shown in Fig 2. The precise degeneracy of the ground states of (3) can be viewed as occurring because both



(a)



(b)

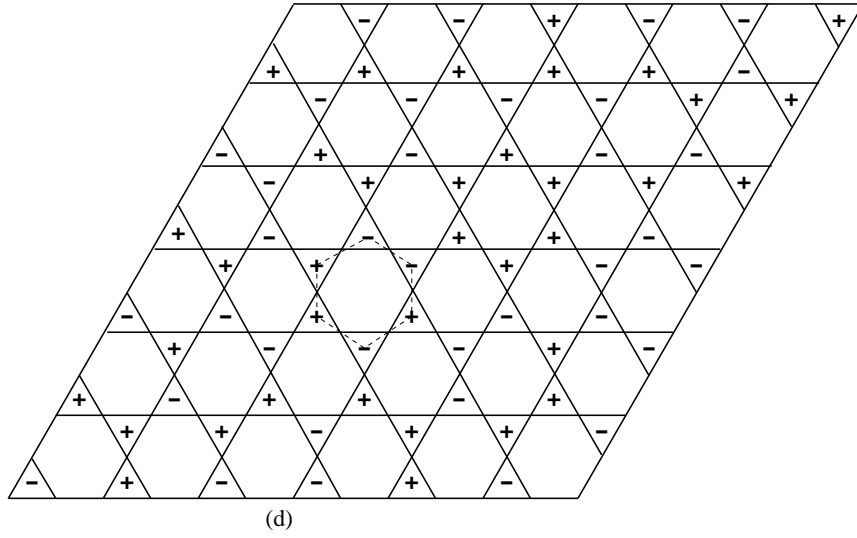
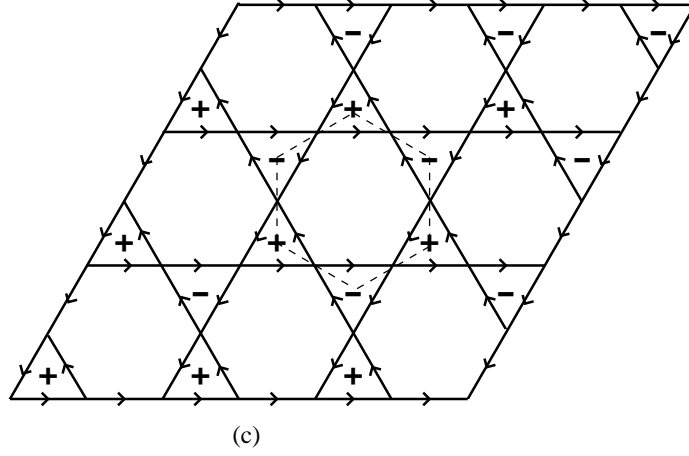


Figure 2: Four minimum energy patterns of a kagome superconducting wire network at $f = 1/2$ in the thin-wire limit. Periodic boundary conditions are applied to the lattices. The arrows represent directions of the supercurrents and + (−) means counterclockwise (clockwise) going supercurrents around triangles. The dotted lines denote unit cell hexagons. (a) the $q = 0$ pattern with (+) triangles only. (b) the $q = 0$ pattern with (−) triangles only. (c) one of the two $\sqrt{3} \times \sqrt{3}$ patterns: the other pattern can be obtained by reversing the directions of all the currents. (d) one of the many disordered current patterns.

(i) each triangle by itself has two degenerate ground states and (ii) there is no interaction energy coupling the directions of the current circulations on different triangles other than the constraint imposed around each hexagon. Effects that we will consider that lift this precise degeneracy are local, so primarily what they do is (i) lift the degeneracy of a single triangle and/or (ii) introduce an interaction between adjacent triangles. Case (i) favors one of the two $q = 0$ patterns (Fig. 2 (a), (b)), where the current circulation has the same sense around every triangle (and necessarily the opposite sense around every hexagon). The $q = 0$ patterns are also selected by an interaction that favors having the same circulation on adjacent triangles. An interaction that favors opposite circulations on adjacent triangles selects the $\sqrt{3} \times \sqrt{3}$ patterns (Fig. 2 (c)). The majority of the minimum-energy current patterns are disordered; we call them “random” patterns. One of the “random” patterns is shown in Fig. 2 (d). There also exist periodic patterns other than the $q = 0$ and $\sqrt{3} \times \sqrt{3}$ patterns. But to stabilize these other periodic patterns, we would need further-neighbor interactions between triangles to be comparable to the single-triangle or nearest-neighbor triangle interactions, which seems unlikely to occur.

If the degeneracy of all these current patterns is not lifted strongly enough, the system will not order into one pattern. Instead it will, by phase-slip processes, move among many patterns, with the equilibrium probability of each pattern being given by its Boltzmann factor. Let us consider the effects of these configurational fluctuations among ground-state current patterns of (3), first neglecting other types of thermal fluctuations of ψ such as vortices or phase fluctuations. Let us consider the phase correlations. If our system does order into one particular current pattern (the most likely candidates being the $\sqrt{3} \times \sqrt{3}$ and $q = 0$ patterns) then if the phase is known at one point on the grid, it is known everywhere. This is the usual situation in a superconducting phase. (Of course, since we are in two dimensions (2d), thermal fluctuations of the phase will reduce this long-range order to power-law quasi-long-range order of ψ and vortices will destroy the superconductivity above a Kosterlitz-Thouless (KT) transition.) Now consider the situation when the system is fluctuating freely among different ground-state current patterns: If the phase is known at one junction of the grid, then we know the gauge-invariant phase change to a neighboring junction is $\pm\pi/3$. Thus the phase there can take on two different values differing by $2\pi/3$. This uncertainty in the phase increases with distance, meaning ψ will not show any long-range order. But there is no uncertainty in $\psi^3 = |\psi|^3 e^{i3\phi}$. Thus even when the system fluctuates freely among the different current patterns it has long-range order in ψ^3 . This is the novel superconducting phase, where Cooper pairs do not show phase coherence at distances large compared to the grid spacing, but “Cooper sextuples” do. Again, since we are in 2d, thermal fluctuations of the phase reduce this to quasi-long-range order, and (fractional) vortices unbind and destroy it at a KT transition. There is another possibility for a superconducting state of this system: it could be out of equilibrium and kinetically frozen in a particular disordered current pattern because the free energy barriers to phase-slip that must be crossed to move among the different patterns are too high compared to the temperature. If the system is in the novel “ ψ^3 ” phase and is cooled to low enough

temperature, this freezing into a sort of kinetic vortex glass state will certainly occur.

If the degeneracy of the current patterns is lifted strongly enough, then the system will be ordered into a conventional ψ ordered phase, either the $\sqrt{3} \times \sqrt{3}$ or $q = 0$ pattern. For the $q = 0$ pattern to be stabilized, we will assume that the energy must be approximately $0.4k_B T$ per unit cell lower than most of the other patterns. This is because the $q = 0$ ordered phase does not have an extensive entropy of circulation patterns, while the allowed patterns have an entropy of roughly $0.4k_B$ per unit cell. When all ground-state current patterns are given the same weight, the system is almost ordered (i.e., has power-law spatial correlations) in the $\sqrt{3} \times \sqrt{3}$ pattern, and a small degeneracy-lifting term favoring the $\sqrt{3} \times \sqrt{3}$ pattern will stabilize that phase.[3] The reason the $\sqrt{3} \times \sqrt{3}$ phase is stabilized so readily is that the system can make local rearrangements of the circulation patterns without destroying the long-range order of this phase, so this phase (unlike the $q = 0$ phase) actually has extensive entropy comparable in magnitude to that of the ψ^3 phase. We have not attempted a more precise statistical-mechanical determination of the phase diagram as a function of the two parameters: the single-triangle degeneracy-lifting term and the nearest-neighbor inter-triangle interaction. Such a study would be of interest and would more precisely delineate when the novel ψ^3 phase is stable.

Among the three possibilities, which superconducting state the system will be in depends on the strength of the degeneracy-lifting effects and the free energy barriers to move vortices at a KT temperature. Above the KT temperature, the superconductivity will be suppressed so there is no ordered phase. Far enough below the KT temperature, because of the large free energy barriers to vortex motion, the system will be kinetically frozen into a particular pattern of ψ (we call this a kinetic vortex glass state) so that experimentally the equilibrium state is not accessible. So in order to explore the three possible superconducting phases, in the following sections, we estimate three things: (i) the helicity modulus of each current pattern to estimate the KT transition temperatures of the ψ ordered phases and the novel ψ^3 ordered phase within the Ginzburg-Landau thin-wire limit, (ii) the amount by which the degeneracy of the current patterns is lifted by various degeneracy-lifting effects (inductive couplings between adjacent supercurrents, non-zero wire width, wire bending, and order-by-disorder effect (thermal fluctuations)), and (iii) the temperature where phase-slip is frozen out due to large barriers to vortex motion.

3 Helicity Modulus

In this section, we estimate the helicity moduli of the different minimum-energy current patterns in order to estimate their Kosterlitz-Thouless (KT) transition temperatures. The free energy cost of a long-wavelength phase distortion [9] is

$$\Delta F = \frac{1}{2} \int d^2 \vec{r} \rho_s(T) (\nabla \delta \phi(\vec{r}))^2, \quad (4)$$

where $\delta\phi$ is the deviation of the phase of the order parameter away from the minimum-free-energy pattern, and $\rho_s(T)$ is the helicity modulus of that pattern. The integral here is over the full two-dimensional space (not just the wires) since the helicity modulus is defined for the continuum approximation to the system. The renormalization group (RG) theory of the KT transition [5] shows that for a conventional superconducting phase, the vortices unbind and the helicity modulus vanishes discontinuously at a KT temperature T_{KT} , with

$$\lim_{T \rightarrow T_{KT}^-} \rho_s(T) = \frac{2}{\pi} k_B T_{KT} . \quad (5)$$

For the ψ^3 phase, on the other hand, the vortices that unbind are $1/3$ -vortices, so attract one another with a potential that is $1/9$ of that for full vortices. Thus the KT criterion for the ψ^3 phase is instead

$$\lim_{T \rightarrow T_{KT,1/3}^-} \rho_s(T) = \frac{18}{\pi} k_B T_{KT,1/3} . \quad (6)$$

We consider the helicity modulus of each minimum-energy current pattern of the thin-wire model. Among all the current patterns, we choose to study the helicity moduli of the two simple patterns: the $q = 0$ and $\sqrt{3} \times \sqrt{3}$ patterns (Fig. 2 (a),(b),(c)). These appear to be the extremal cases, with the helicity moduli of other patterns being intermediate between these two. Our analysis shows that the $\sqrt{3} \times \sqrt{3}$ pattern has a smaller helicity modulus than the $q = 0$ pattern, and that the helicity moduli of all current patterns become identical in the London limit of $\xi_0 \ll a$.

When a long-wavelength distortion of the phase of the order parameter is applied to a particular minimum-energy current pattern, within Ginzburg-Landau theory we have to take into account the distortion of the magnitude of the order parameter as well as that of the phase. In the London limit these magnitude distortions are negligible. But we find that near the mean-field transition temperature, the effect on the helicity modulus due to magnitude distortions is substantial. If we write the magnitude distortion as $\delta|\psi|$ and the phase distortion as $\delta\phi$, the distortion of the complex order parameter $\delta\psi$ will be, up to first order in $\delta|\psi|$ and $\delta\phi$,

$$\delta\psi = (\delta|\psi| + i|\psi_0|\delta\phi)e^{i\phi_0} , \quad (7)$$

where $|\psi_0|$ and ϕ_0 represent the minimum energy magnitude and phase of the order parameter in the particular ψ pattern being considered. The difference between the (thin-wire) GL free energies with and without the distortion is, up to second order in $\delta|\psi|$ and $\delta\phi$,

$$\begin{aligned} F[\psi_0 + \delta\psi] - F[\psi_0] = & \quad wd \int ds [2|\psi_0|^2(\delta|\psi|)^2 + \xi_0^2(\nabla\delta|\psi|)^2 \\ & + \xi_0^2|\psi_0|^2(\nabla\delta\phi)^2 + 4\xi_0^2|\psi_0|(\nabla_g\phi_0 \cdot \nabla\delta\phi)\delta|\psi|] , \end{aligned} \quad (8)$$

where $|\nabla_g\phi_0| = \pi/3$. The term $(\nabla_g\phi_0 \cdot \nabla\delta\phi)\delta|\psi|$ couples amplitude and phase and will be negative to minimize the free energy cost of any spatially nonuniform phase distortion.

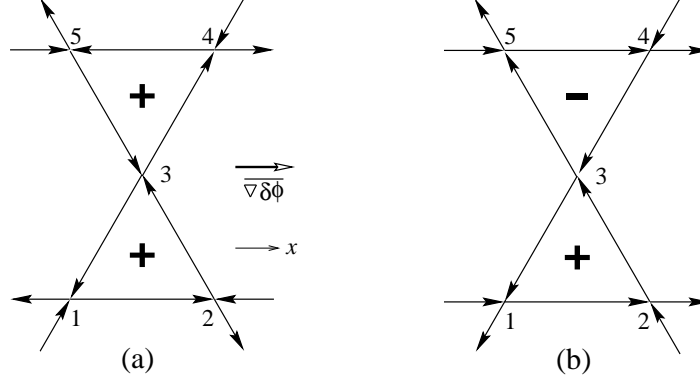


Figure 3: Gauge-invariant unit cells of the $q = 0$ (a) and $\sqrt{3} \times \sqrt{3}$ pattern (b). Arrows represent the supercurrents. The junctions are marked by numbers. The small large-scale average phase gradient $\overline{\nabla \delta \phi}$ added to measure the helicity moduli is along the x direction.

Without the magnitude distortion (i.e. for $\delta|\psi| = 0$), one can see from (8) that the helicity modulus does not depend on the current pattern; this is the result in the London limit.

Minimizing the free energy difference with respect to the order parameter magnitude and phase, we obtain the (Euler-Lagrange) equations that apply along each wire segment:

$$2|\psi_0|^2 \delta|\psi| + 2\xi_0^2 |\psi_0| \nabla_g \phi_0 \cdot \nabla \delta\phi - \xi_0^2 \nabla^2 \delta|\psi| = 0, \quad (9)$$

$$2\nabla_g \phi_0 \cdot \nabla \delta|\psi| + |\psi_0| \nabla^2 \delta\phi = 0. \quad (10)$$

For the current patterns of interest, these equations are homogeneous and linear, so are straightforwardly solved for each wire segment. The boundary conditions at the junctions are that $\delta|\psi|$ and $\delta\phi$ are continuous and that the sums of the first derivatives of $\delta|\psi|$ and $\delta\phi$ moving away from each junction i along each of the 4 wire segments meeting at that junction must vanish:

$$\sum_{j=1}^4 \nabla_{ij} \delta|\psi|_i = 0, \quad \sum_{j=1}^4 \nabla_{ij} \delta\phi_i = 0, \quad (11)$$

where ∇_{ij} denote the derivative taken with the position coordinate increasing as one moves from junction i to neighboring junction j . The supercurrents are conserved if all the above conditions are satisfied.

Fig. 3 shows the gauge-invariant unit cells of the two current patterns that we examine. For the purpose of the present discussion, we choose the unit cell to consist of two adjacent triangles (elsewhere we use a single hexagon as an alternative unit cell). To calculate the helicity modulus, we apply a small added phase gradient that is uniform at scales larger than a unit cell, with a spatial average of $\overline{\nabla \delta \phi}$. With this gradient the new minimum free

energy state has a pattern of the gauge-invariant variables $\delta|\psi|$ and $\nabla\delta\phi$ that is the same in every unit cell, but $\delta\phi$ changes systematically between cells:

$$\delta|\psi|(\vec{r} + \vec{R}) = \delta|\psi|(\vec{r}) , \quad (12)$$

$$\nabla\delta\phi(\vec{r} + \vec{R}) = \nabla\delta\phi(\vec{r}) , \quad (13)$$

$$\delta\phi(\vec{r} + \vec{R}) = \delta\phi(\vec{r}) + \vec{R} \cdot \overline{\vec{\nabla}\delta\phi} , \quad (14)$$

where \vec{R} is any lattice translation vector connecting equivalent points in two different unit cells. Along each wire segment, the added phase gradient $\nabla\delta\phi$ is either of the same or opposite sign from the gauge-invariant phase gradient $\nabla_g\phi_0$ that is already present. This results in a change in the magnitude of the supercurrent, and a resulting decrease or increase, respectively, in $|\psi|$. For our two patterns the helicity modulus is isotropic. Let us put the added phase gradient along the x direction, as illustrated in Fig. 3. Let us look at what happens in the vicinity of junction 3 in Fig. 3. For the $q = 0$ pattern (Fig. 3 (a)), the added phase gradient increases the supercurrent in two of the adjoining wires, while it decreases it in the other two. The net effect is that, to lowest order in the added phase gradient, $\delta|\psi| = 0$ at the junction. This is true at all the junctions for the $q = 0$ pattern for any orientation of the added phase gradient. For the $\sqrt{3} \times \sqrt{3}$ pattern (Fig. 3 (b)), on the other hand, the added phase gradient decreases the supercurrent on all the wires adjacent to junction 3, and therefore increases $|\psi|$ at that junction. A decrease in $|\psi|$ also occurs at the other two junctions. This additional “relaxation” of $|\psi|$ at the junctions is connected with a lower free energy cost of the added phase gradient and thus a lower helicity modulus in the $\sqrt{3} \times \sqrt{3}$ pattern than in the $q = 0$ pattern.

From the definition of the helicity modulus (4), the energy cost per unit cell due to the added phase distortion is

$$\Delta F = A_{hex} \frac{1}{2} \rho_s(T) (\overline{\vec{\nabla}\delta\phi})^2 , \quad (15)$$

where $A_{hex} = 2\sqrt{3}a^2$ is the area of a unit cell. We have obtained the helicity moduli of both patterns at all temperatures. The results simplify near the mean-field phase transition where, surprisingly, the helicity modulus of the $\sqrt{3} \times \sqrt{3}$ pattern, $\rho_s[\sqrt{3} \times \sqrt{3}]$, vanishes much faster than that of the $q = 0$ pattern, $\rho_s[q = 0]$, as $|\psi_0| \rightarrow 0$. For $|\psi_0| \ll 1$ we obtain

$$\rho_s[q = 0] \approx |\psi_0|^2 E_c / \pi , \quad (16)$$

$$\rho_s[\sqrt{3} \times \sqrt{3}] \approx \frac{2}{3\sqrt{3}} |\psi_0|^4 E_c , \quad (17)$$

where

$$E_c \equiv \frac{3H_c^2}{4\pi} w \cdot d \cdot a \quad (18)$$

is the condensation energy per unit cell in zero field. Note that E_c remains nonzero at the $f = 1/2$ transition temperature. At low temperature in the London regime where $\xi_0 \ll a$, the magnitude distortions are negligible and the the helicity moduli of all of the current patterns are $\rho_s \approx 2(\xi_0/a)^2 E_c/\sqrt{3}$. More generally, the helicity moduli are

$$\rho_s[\sqrt{3} \times \sqrt{3}] = \frac{E_c}{2\sqrt{3}} \frac{\xi_0^4 \eta^2 \left(\frac{2\cos\eta+1}{\sin\eta}\right)}{\frac{6(\nabla_g \phi_0)^2}{|\psi_0|^2 \eta} \xi_0^2 - \left(\frac{2\cos\eta+1}{\sin\eta}\right)}, \quad (19)$$

$$\rho_s[q=0] = \frac{E_c}{2\sqrt{3}} \frac{\xi_0^4 \eta^2}{\frac{4(\nabla_g \phi_0)^2}{|\psi_0|^2 \eta} \xi_0^2 \left(\frac{1-\cos\eta}{\sin\eta}\right) - 1}, \quad (20)$$

$$\frac{\eta^2}{2} \equiv 3(\nabla_g \phi_0)^2 - \xi_0^{-2},$$

where the temperature dependence is in ξ_0 , $|\psi_0|$, η , and E_c .

These helicity moduli can be used to estimate the Kosterlitz-Thouless (KT) transition temperatures of the various possible phases. Putting in the experimental parameters from Appendix A we obtain for the conventional ψ ordered phases $1 - \frac{T_{KT, \sqrt{3} \times \sqrt{3}}(f=\frac{1}{2})}{T_c^m(f=\frac{1}{2})} \approx 0.0017$ and $1 - \frac{T_{KT, q=0}(f=\frac{1}{2})}{T_c^m(f=\frac{1}{2})} \approx 0.0007$. Note that the KT transition temperature is lower for the $\sqrt{3} \times \sqrt{3}$ phase because of its smaller helicity modulus. Stability of the novel ψ^3 phase requires a nine time larger helicity modulus, so this phase's KT transition occurs at lower temperature. For our parameters it is in the crossover between GL and London regimes, where the difference in helicity moduli between patterns is not very large. Because the random current patterns are locally more similar to the $\sqrt{3} \times \sqrt{3}$ patterns than they are to the $q=0$ patterns, we will use the helicity modulus of the $\sqrt{3} \times \sqrt{3}$ pattern (19) to estimate the KT transition of the ψ^3 phase. This leads to $1 - \frac{T_{KT, 1/3}(f=\frac{1}{2})}{T_c^m(f=\frac{1}{2})} \approx 0.007$.

4 Degeneracy-Lifting Effects

Now that we have estimated the KT temperatures of the ψ ordered phases and the ψ^3 ordered phase, in this section we consider effects that lift the degeneracy of the minimum energy patterns at $f = 1/2$, estimating the strength of each effect at the KT temperatures. The net result of these effects determines which of the possible superconducting phases occur in this system. First we consider the inductive coupling between the supercurrents in different triangles, finding that this effect is negligible near the KT transitions for the experimental parameters we consider. The effects that can substantially lift the degeneracy are the nonzero width of the wires, a possible bending of the wires away from straight, and “order-by-disorder” effects due to thermal fluctuations in the Ginzburg-Landau regime.

4.1 Magnetic Energy

One effect that lifts the degeneracy of the ground-state current patterns in the thin-wire limit of mean-field theory is the magnetic energy due to the inductance of the grid and the supercurrents. Here we estimate this effect, finding that it is quite small at the KT transition for parameters corresponding to the recent experiments [6][7]. Since the magnitudes of the currents flowing in every triangle are identical, the energy due to self-inductance of each triangle is the same for every current pattern. The energy due to mutual inductance [10] is

$$F_m = \frac{1}{2} \sum_{i \neq j} M_{ij} I_i I_j, \quad (21)$$

$$M_{i,j} = \frac{1}{c^2} \oint_{C_i} \oint_{C_j} \frac{d\vec{l}_i \cdot d\vec{l}_j}{|\vec{r}_i - \vec{r}_j|}, \quad (22)$$

where M_{ij} is the mutual inductance between triangles i and j and I_i is the supercurrent in triangle i . C_i is the closed contour around the i th triangle. At large distance r , the interaction is a magnetic dipole-dipole coupling, so falls off as r^{-3} , making the sum well-convergent. In fact, the interaction between nearest-neighbor triangles is dominant in the sum. If only nearest-neighbor pairs of triangles are included, $F_m(\sqrt{3} \times \sqrt{3}) - F_m(q=0) \cong 0.53 \frac{aI^2}{c^2}$. (The second and third neighbor contributions are an order of magnitude smaller at $0.052 \frac{aI^2}{c^2}$ and $0.032 \frac{aI^2}{c^2}$, respectively.) Thus the $q=0$ pattern has the lowest magnetic energy.

The magnetic energy difference per unit cell for our experimental parameters (Appendix A) is approximately $50k_B T_c (1 - \frac{T}{T_c^m(f=1/2)})^2$. Since $(1 - \frac{T_{KT,1/3}(f=1/2)}{T_c^m(f=1/2)})$ is about 0.007, the magnetic energy difference is about $0.002k_B T_c$ at $T_{KT,1/3}$, which is negligible compared to the other degeneracy-lifting effects that we examine below.

4.2 Finite Wire Width

So far, we have assumed that the wires can be considered as perfect mathematical lines and the junctions as perfect points. In real experiments, the wires have a non-zero width w , and the supercurrent density is nonuniform across the width of the wires and at the junctions. In this section, we estimate how much this non-zero wire width lifts the degeneracy of the minimum energy current patterns. The degeneracy of the two ground states of a single triangle is lifted, favoring the $q=0(--)$ pattern. Here we assume that the wires are straight, as in the published experiment [7].

As a simple model for a rough description and estimate of this effect, let us approximate a single triangle as a circle, and ignore its connections to the other triangles. Below we treat the kagome grid numerically to check when this crude model is qualitatively correct. The model we use is a circular wire loop of width w , occupying the area between concentric circles of radii $1 - w/2$ and $1 + w/2$. The uniform applied field is such that one-half of a

flux quantum passes through the circle whose perimeter runs along the center of the wire. The two nearly-degenerate current patterns both have supercurrents flowing only around the loop, so the gauge-invariant phase gradient $\vec{\nabla}_g \phi$ has no radial component; the currents flow in opposite directions in the two patterns. The $(-)$ pattern has no vortex within the loop, and has

$$|\nabla_g \phi_-| = \frac{r}{2}, \quad (23)$$

at radius r . The $(+)$ pattern has a vortex within the loop, resulting in

$$|\nabla_g \phi_+| = \frac{1}{r} - \frac{r}{2}. \quad (24)$$

The energies $E_L^{(\pm)}$ of these supercurrents are readily obtained in the London approximation. The $(-)$ pattern has the lower energy. For $w \ll a$ the energy difference is of order $(w/a)^2 E_L$. We verify below that this simple argument provides the correct sign and order in (w/a) of the energy difference, but the coefficient of the leading term is not estimated accurately with this rough model. This is because in the proper kagome geometry the details of the current patterns around the junctions that have been ignored in this crude model contribute substantially to the small energy difference. The essential conclusion here is that the lowest energy pattern has the vortices in the hexagons and not in the triangles.

We can go one step further with this simple model, and estimate the energies in Ginzburg-Landau theory instead of the London approximation. For $w \ll a$ the relative variation of the order parameter magnitude across the wires is only of order $(w/a)^3$, and the resulting Ginzburg-Landau contribution to the energy difference is of order $(w/a)^4 E_L$, and thus only a small correction to the result from the London approximation for the relatively narrow wires we are interested in. We have numerically obtained the minimum free energy order parameter patterns within Ginzburg-Landau theory on the proper kagome lattice to verify that we are indeed justified in using the simpler London approximation [11].

The London energy that we consider is

$$F_L = d \xi_0^2 |\psi_0|^2 \int d\mathcal{A} (\vec{\nabla} \phi - \vec{A})^2, \quad (25)$$

where the integral runs over the area occupied by the wires, as illustrated in Fig. 4. We obtain the London energy of the $\sqrt{3} \times \sqrt{3}$ pattern and of the two different $q = 0$ patterns. Each of these current patterns has a high symmetry, so we need to solve for the pattern only in a small fraction of the unit cell, as indicated in Fig. 4. We discretize the system with an equilateral triangular numerical grid where nearest-neighbor grid vectors are aligned parallel to the edges of the wires. We represent the patterns in terms of gauge-invariant phase differences only. The uniform magnetic field induces net diamagnetic currents circulating around each elementary plaquette of our numerical grid. In each pattern the gauge-invariant phase difference between the centers of adjacent wire

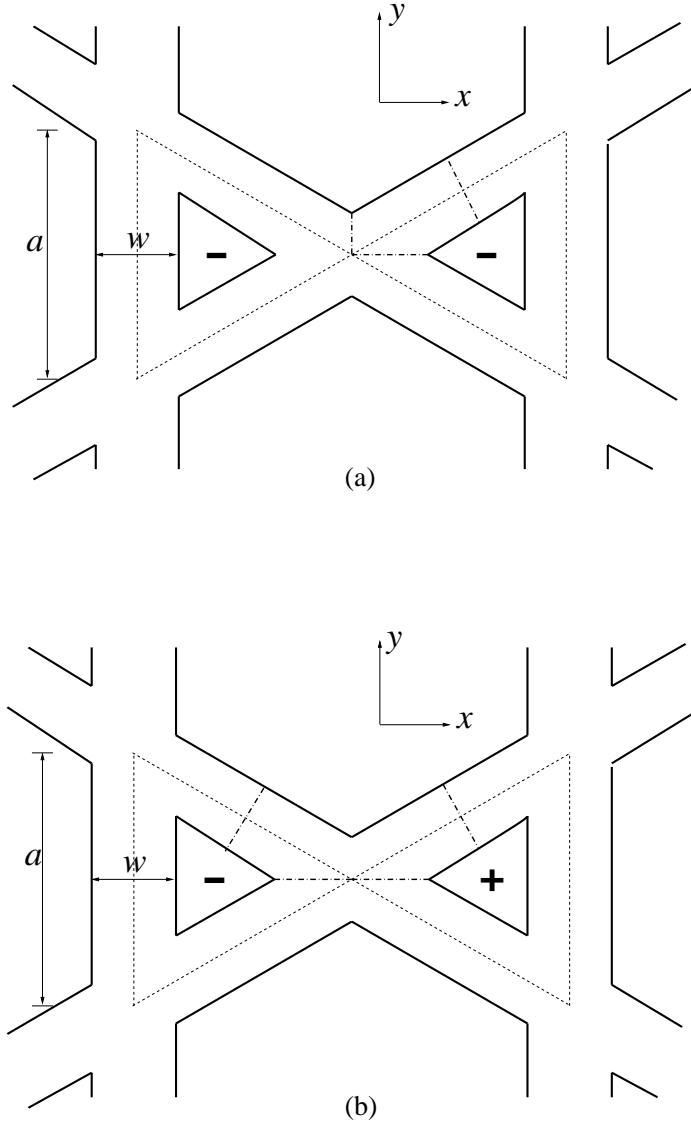


Figure 4: Part of the kagome-lattice wire network with non-zero wire width w . (For clarity, the wire width is shown larger than the values $w/a \approx 0.1$ examined in the recent experiments.) A half of one flux quantum penetrates through each of the triangles surrounded by the dotted lines along the centers of the wires. Because of the symmetries of the order parameter and supercurrent patterns, we need to solve for the patterns only in the areas confined by the dash-dotted lines and the boundaries of the wires. (a) In the $q = 0$ patterns, only one twelfth of a unit cell is needed. (b) In the $\sqrt{3} \times \sqrt{3}$ pattern, only one sixth of a unit cell is needed.

Table 1: London energy and energy differences between the different current patterns in units of $E_L \equiv 2(\frac{\xi_0}{a})^2 |\psi_0|^2 (\pi/3)^2 E_c$ for various wire widths. F_{++} , F_{--} , and F_{-+} denote the London energy per unit cell for the $q = 0(++)$, $q = 0(--)$, and $\sqrt{3} \times \sqrt{3}$ patterns, respectively.

w/a	F_{++}	F_{--}	F_{-+}	$F_{++} - F_{--}$	$F_{++} - F_{-+}$	$F_{-+} - F_{--}$
0.0201	1.02344	1.02091	1.02049	0.00253	0.00295	-0.00042
0.0422	1.05662	1.04680	1.04831	0.00982	0.00831	0.00151
0.0619	1.09615	1.07465	1.08018	0.0215	0.01597	0.00553
0.0825	1.14494	1.10582	1.11804	0.03912	0.0269	0.01222
0.1019	1.19840	1.13736	1.15836	0.06104	0.04004	0.021
0.1237	1.26741	1.17495	1.20899	0.09246	0.05842	0.03404

junctions along the center line of the connecting wire is fixed to be $\pm\pi/3$ depending on the direction of the supercurrents. For each grid spacing we use, we put as many grid points as possible along all boundaries.

For each pattern we start with physically-sensible smooth initial conditions that satisfy the above constraints. Then we minimize the discretized version of the London energy for the $q = 0(++)$, $q = 0(--)$, and $\sqrt{3} \times \sqrt{3}$ patterns using the relaxation method. We have done this for various values of the normalized wire width, w/a . For each wire width, we use various different grid spacings. We then use these results for different grid spacings to extrapolate to the continuum limit. [11]

Our results for this non-zero wire width effect are presented in Table 1. Except for extremely thin wires, the $q = 0(--)$ pattern has the lowest energy, F_{--} , and the energy of the $q = 0(++)$ pattern, F_{++} , is higher by of order $(w/a)^2 E_L$, consistent with our crude “circle” model. If all that were happening is simply a lifting of the degeneracy of the single-triangle energy then the $\sqrt{3} \times \sqrt{3}$ pattern, with equal numbers of (+) and (−) triangles, would have an energy $(F_{++} - F_{--})/2$. Instead we find that F_{-+} is a little lower than this, indicating that the non-zero wire width also generates an interaction between the triangles that favors the $\sqrt{3} \times \sqrt{3}$ pattern. For wire widths near those of the experiments, the single-triangle effect dominates over this interaction, but for very narrow wires, $w/a \cong 0.02$, the $\sqrt{3} \times \sqrt{3}$ pattern seems to have lower energy than the $q = 0(--)$ pattern. We have not found an analytical understanding of this result for very thin wires. It is somehow due to the nontrivial current pattern near the wire junctions.

For the experimental wire width of $w = 0.1a$, we see from Table 1 that the non-zero wire width lowers the free energy of the $q = 0(--)$ pattern by roughly $0.02E_L$ compared to a $\sqrt{3} \times \sqrt{3}$ or random pattern. For the experimental parameters we are using (Appendix A), the London energy per unit cell is roughly $E_L \cong 5000k_B T_c (1 - \frac{T}{T_c^{m(f=1/2)}})$. Thus if

this were the only degeneracy-lifting effect, it would overcome the roughly $0.4k_B$ entropy difference per unit cell and stabilize the conventional $q = 0(--)$ superconducting phase at $(1 - \frac{T}{T_c^m(f=1/2)}) \cong 0.004$. This is below that phase's KT temperature, so it would be also stable against vortices. And this is above the KT temperature of the ψ^3 ordered phase, so the system will not enter this latter novel superconducting phase unless either this non-zero wire width effect is reduced by making the wires narrower or changing the experimental parameters or it is counterbalanced by some other effect. What appears to be the simplest way of counterbalancing this effect is to bend the wires slightly away from straight, while maintaining the full symmetry of the kagome grid, as is discussed below.

4.3 Order-by-Disorder

Another effect we consider that lifts the degeneracy in the minimum-energy current patterns is the thermal fluctuations of ψ around the minimum-energy patterns. This effect is called “order-by-disorder” [12][13][14]. For the *kagome* antiferromagnet XY spin model (1) with nearest neighbor interaction and fixed-length spins, thermal fluctuations do not lift the degeneracy in the ground states [3] because they produce only phase fluctuations and these fluctuations are, at lowest order, the same for all ground states. But in our kagome-lattice superconducting wire network, the magnitude of the order parameter can also fluctuate, and the free energy of these thermal fluctuations does lift the degeneracy among the current patterns in the Ginzburg-Landau regime near T_c .

To estimate the effect of thermal fluctuations, we expand the energy of the system around the minimum-energy states, where $\frac{\delta F[\psi]}{\delta \psi^*} = 0$, to quadratic order in the fluctuations. The difference between the GL thin-wire limit free energy with and without fluctuations is given by (8). (We treat the fluctuations only in the thin-wire limit.) Because of the coupling term between the magnitude and the phase fluctuations, the energy of a given fluctuation generally depends on the current pattern. This is why the degeneracy in the minimum-energy current patterns can be lifted by thermal fluctuations. Linearizing, the eigenmode i of the fluctuations satisfies

$$\frac{\delta F[\delta \psi_i]}{\delta(\delta \psi_i^*)} = \Gamma_i \delta \psi_i, \quad (26)$$

where Γ_i is the stiffness of that eigenmode i . We will focus on the soft modes, with small stiffnesses, because these are the modes that have substantially different stiffnesses in the different patterns, thus lifting the degeneracy. To lowest order in the amplitude of the fluctuations, their contribution to the free energy is

$$\Delta F = \sum_i \frac{k_B T}{2} \log \Gamma_i \quad (27)$$

(ignoring an additive constant which does not depend on the current pattern). The sum runs over all eigenmodes of the fluctuations. Like the other effects, we estimate this effect

for the two extremal cases only: the $q = 0$ and $\sqrt{3} \times \sqrt{3}$ patterns. Using the free energy difference (8) and equation (26), we obtain the eigenvalue equations for the magnitude $\delta|\psi|_i$ and the phase $\delta\phi_i$ of the fluctuations in eigenmode i :

$$\Gamma_i \delta|\psi|_i = 4|\psi_0|^2 \delta|\psi|_i + 4\xi_0^2 |\psi_0| \nabla_g \phi_0 \cdot \nabla \delta\phi_i - 2\xi_0^2 \nabla^2 \delta|\psi|_i , \quad (28)$$

$$\Gamma_i |\psi_0| \delta\phi_i = -4\xi_0^2 \nabla_g \phi_0 \cdot \nabla \delta|\psi|_i - 2\xi_0^2 |\psi_0| \nabla^2 \delta\phi_i . \quad (29)$$

These equations apply along each wire segment. The boundary conditions at each junction are that $\delta|\psi|_i$ and $\delta\phi_i$ are continuous, and that the sums of the first derivatives of $\delta|\psi|_i$ and $\delta\phi_i$ moving away from each junction along each of the four wire segments meeting at that junction must both vanish.

For a thermal fluctuation with crystal momentum \vec{Q} , Bloch's theorem says

$$\delta|\psi|(\vec{r} + \vec{R}) = e^{i\vec{Q} \cdot \vec{R}} \delta|\psi|(\vec{r}) , \quad (30)$$

$$\nabla \delta\phi(\vec{r} + \vec{R}) = e^{i\vec{Q} \cdot \vec{R}} \nabla \delta\phi(\vec{r}) , \quad (31)$$

where \vec{R} is any lattice translation vector connecting equivalent points in two different unit cells. Using the equations (30) and (31), we can write the boundary conditions for the first derivatives of $\delta|\psi|$ and $\delta\phi$ at each junction in a unit cell as an eigenvalue equation with eigenvalue Γ :

$$G_{\vec{Q}}(\Gamma)[\delta\psi] = 0 , \quad (32)$$

where $G_{\vec{Q}}(\Gamma)$ is a 6×6 matrix depending in a nontrivial way on the eigenvalue $\Gamma(\vec{Q})$, and $[\delta\psi(\vec{Q})]$ is a column vector that consists of $\delta|\psi|$ and $\delta\phi$ at each of the three junctions in a unit cell. Our goal is to solve this eigenvalue equation for small $\Gamma(\vec{Q})$ at all points in the first Brillouin Zone (BZ) (Fig. 5). In general, this is not possible to do analytically, so we must solve for the fluctuation spectrum numerically. However, near the mean-field transition temperature where $|\psi_0|$ is small we can obtain some analytic results that are perturbative in $|\psi_0|$.

At the mean-field transition temperature

At the mean-field transition temperature $T = T_c^m(f = 1/2)$ there is only one order parameter pattern that minimizes the GL free energy, namely the normal state, with $\psi = 0$ everywhere. Here we can not solve for the fluctuation eigenmodes in the gauge-invariant fashion discussed above, because the phase ϕ is everywhere ill-defined. However, it is fairly straightforward to solve for the modes by choosing a convenient gauge to work in. [11] We find at $T_c^m(f = 1/2)$ that the fluctuations have a complex zero-mode, with stiffness $\Gamma_i = 0$, over the entire first Brillouin zone. Since this zero mode is complex, it represents two real modes that will each acquire a stiffness as soon as $|\psi_0|$ is increased from zero by decreasing T below $T_c^m(f = 1/2)$. The other modes all have stiffnesses of order one, except at isolated

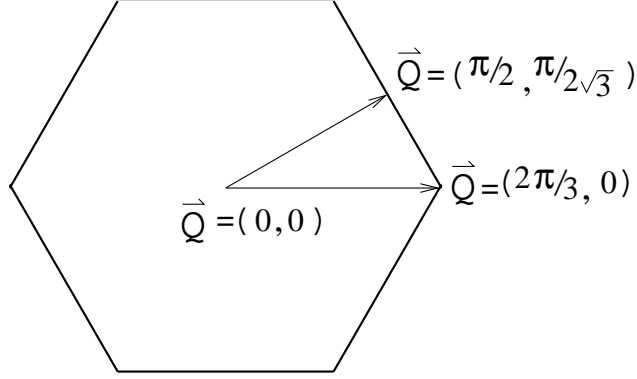


Figure 5: First Brillouin zone of the kagome lattice.

points in the zone. In the GL limit of $|\psi_0| \ll 1$, it is only the lowest two soft modes that contribute to the order-by-disorder effect that lifts the degeneracy between current patterns, because the higher modes have stiffnesses that do not depend on the patterns to lowest order in $|\psi_0|$.

In the limit $|\psi_0| \rightarrow 0$

When temperature decreases from the mean-field transition temperature, the two degenerate zero modes that are present over the entire first Brillouin zone for all current patterns acquire stiffnesses of order $|\psi_0|^2$. The modes at a given \vec{Q} acquire stiffnesses that depend on the current pattern. Now we will examine these two lowest modes in order to estimate the free energy difference between the $q = 0$ and $\sqrt{3} \times \sqrt{3}$ patterns in this limit.

To obtain the stiffnesses of the soft modes with general momentum \vec{Q} we expand the elements of our matrix $G_{\vec{Q}}(\Gamma)$ (32) to lowest order in $|\psi_0|$ for general \vec{Q} , using the fact that the stiffnesses of interest are themselves of order $|\psi_0|^2$. The stiffnesses of the two soft modes for the two patterns are, to lowest order in $|\psi_0|$,

$$\Gamma_{\pm}[\sqrt{3} \times \sqrt{3}] \approx 2|\psi_0|^2 \left[1 \pm \sqrt{1 - \frac{6(3-w)}{33+16u+2v-2w}} \right], \quad (33)$$

$$\Gamma_{\pm}[q=0] \approx 2|\psi_0|^2 \left[1 \pm \sqrt{1 - \frac{3(6-3u+w)}{21-10u+v+2w}} \right]; \quad (34)$$

$$\begin{aligned} u &\equiv \cos(Q_x + \sqrt{3}Q_y) + \cos(2Q_x) + \cos(Q_x - \sqrt{3}Q_y), \\ v &\equiv \cos(2(Q_x + \sqrt{3}Q_y)) + \cos(4Q_x) + \cos(2(Q_x - \sqrt{3}Q_y)), \\ w &\equiv \cos(3Q_x + \sqrt{3}Q_y) + \cos(2\sqrt{3}Q_y) + \cos(3Q_x - \sqrt{3}Q_y). \end{aligned}$$

Because they are obtained ignoring the higher modes, these analytic expressions for the

Table 2: Stiffnesses of the four softest modes for the $q = 0$ and $\sqrt{3} \times \sqrt{3}$ patterns at symmetry points in the first BZ at the KT temperature of the ψ^3 phase for our experimental parameters. All modes are obtained numerically. The degeneracy of the modes are indicated in parentheses when they are degenerate.

\vec{Q}	$\Gamma[q = 0]$	$\Gamma[\sqrt{3} \times \sqrt{3}]$
(0,0)	0, 1.02 (2), 2.7	0, 1.79 (2), 2.7
$(\frac{\pi}{2}, \frac{\pi}{2\sqrt{3}})$	0.35, 1, 1.4, 2.9	0.47, 0.7, 1.16, 2.8
$(\frac{2\pi}{3}, 0)$	0.62 (2), 1.79, 3.	0.62 (2), 1.02, >3.

stiffnesses are not valid at all \vec{Q} : For the $q = 0$ pattern the behavior is different at $\vec{Q} = 0$, where there are actually 4 soft modes. For the $\sqrt{3} \times \sqrt{3}$ pattern, there is a third soft mode at each of the corners of the Brillouin zone. However, in obtaining the order-by-disorder effect to lowest order in $|\psi_0|$, these isolated special points in the zone may be ignored, since they do not contribute to the full free energy at that order.

The lowest-order fluctuation contribution to the free energy per unit cell from the two soft modes is (again, ignoring an additive constant that is independent of the current pattern)

$$\Delta F \approx \frac{k_B T}{2} \frac{A_{hex}}{(2\pi)^2} \int d^2 Q (\log \Gamma_+(\vec{Q}) + \log \Gamma_-(\vec{Q})) . \quad (35)$$

In the limit of small $|\psi_0|$ the resulting contribution to the free energy difference between our two current patterns is

$$\Delta F_{\sqrt{3} \times \sqrt{3}} - \Delta F_{q=0} \cong \frac{\sqrt{3}}{(2\pi)^2} (-3.68) k_B T \cong -0.16 k_B T . \quad (36)$$

Thus in this limit there is a nonzero order-by-disorder effect, with the $\sqrt{3} \times \sqrt{3}$ pattern having the lower free energy.

Intermediate region

As the temperature is reduced, the order-by-disorder effect also decreases, and it vanishes in the low-temperature London limit of $\xi_0 \ll a$. With our experimental parameters (Appendix A), the KT temperature of the ψ^3 phase falls in the crossover regime between Ginzburg-Landau and London regimes. Here we have to solve the eigenvalue equation (32) numerically for the stiffnesses $\Gamma(\vec{Q})$ of the fluctuation modes with the experimental parameters. Table 2 shows the four softest modes at symmetry points in the first BZ; we obtained

these stiffnesses throughout the Brillouin zone. We found that the free energy difference between the two patterns is predominantly due to the lowest three modes. The resulting order-by-disorder contribution to the free energy difference per unit cell between the $\sqrt{3} \times \sqrt{3}$ and $q = 0$ patterns is roughly $0.04k_B T$ at the KT temperature of the ψ^3 ordered phase, with the $\sqrt{3} \times \sqrt{3}$ pattern still having the lower fluctuation free energy. Note that this is indeed substantially lower than the roughly $0.16k_B T$ difference near the mean-field transition. Note also that at this KT transition the order-by-disorder effect is also much smaller than the finite-wire width effect discussed above, so it is too weak to cause the novel ψ^3 superconducting phase to be stabilized.

4.4 Bending of the Wires

From the previous two subsections, we know that the effect of the non-zero wire width is dominant over the order-by-disorder effect at the KT transition of the ψ^3 ordered phase for the experimental parameters, so the system orders into the $q = 0(- -)$ pattern when the wire segments are straight. However, the novel ψ^3 superconducting phase might be stabilized by bending the wires away from straight to counteract the non-zero wire width effect.

Let us consider a possible bending of the wires away from straight while maintaining all translational and rotational symmetries of the kagome grid. We have been calling the magnetic field of interest $f = 1/2$, meaning one half of a flux quantum through each triangle. We consider wire bending that changes the area of a triangle, while not changing the area of a full unit cell. Thus once we bend the wires, the magnetic field of interest is more precisely specified as being four flux quanta per unit cell. We consider bending the wires by a distance ϵ , while keeping the junctions at their original locations, as illustrated in Fig. 6. The junctions are points of symmetry of the grid, which is why they must stay put. This wire-bending lifts the degeneracy of the two ground states of a single triangle. The free energy of the $(-)$ pattern is lowered when the wires are bent in towards the interior of the triangle, and is increased when they are bent out as in Fig. 6 (b). Since the nonzero wire width stabilizes the $q = 0(- -)$ pattern, we are interested in bending the wires out in order to destabilize it and allow the system to order into the ψ^3 superconducting phase.

To analyze this quantitatively, we must assume some shape for the bent wire segments. For concreteness, let us assume they are arcs of constant curvature. Then the extra area of the triangle due to the bending is simply $2a\epsilon$, to lowest order in ϵ . (Negative ϵ corresponds to bending the wires in.)

The resulting gauge-invariant phase gradients on the $(+)$ and $(-)$ triangles $|\nabla_g \phi_0^{(\pm)}|$ are, to first order in ϵ/a ,

$$|\nabla_g \phi_0^{(\pm)}| \approx \frac{\pi}{3a} \left(1 \mp \frac{8\epsilon}{\sqrt{3}a} \right). \quad (37)$$

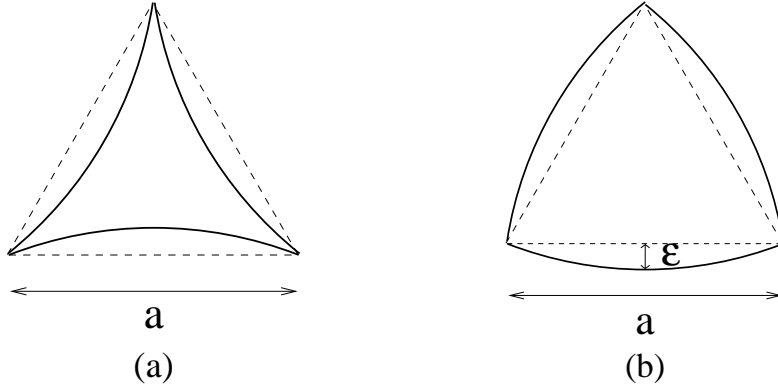


Figure 6: Elementary triangles with the wires bent (a) in towards the center of the triangle and (b) out away from the triangle. The straight lines between junctions are shown dashed.

This results in a Ginzburg-Landau energy difference between the two patterns of

$$E^{(+)} - E^{(-)} \approx -\frac{16\epsilon}{\sqrt{3}a} E_L. \quad (38)$$

Bending the wires does not affect the energy of the $\sqrt{3} \times \sqrt{3}$ pattern at order ϵ/a . For the experimental parameters (Appendix A), to fully counteract the non-zero wire width effect listed in Table 1 and bring the $q = 0(--)$ and $q = 0(++)$ patterns back to degeneracy requires a surprisingly small bend of $\epsilon \cong 70\text{\AA}$. With this ϵ , the $\sqrt{3} \times \sqrt{3}$ pattern has the lowest free energy, mostly due to the non-zero wire width effect, with the order-by-disorder effect also contributing. For a smaller bend of roughly 20 to 50 \AA , the $q = 0(--)$ pattern still has the smallest energy, but by less than $0.4k_B T$; here we expect the ψ^3 phase to be stabilized. If the bend is increased beyond about 90 \AA , the $q = 0(++)$ pattern becomes the lowest energy. Up to about 120 \AA , the difference in energy between the $q = 0(++)$ and $\sqrt{3} \times \sqrt{3}$ patterns is too small to stabilize the $q = 0(++)$ pattern and again we expect the ψ^3 phase to be stable. Then the $q = 0(++)$ phase is stabilized for even larger bends. Thus it appears that any of the superconducting phases we have discussed can be stabilized near the phase transition by making quite small bends in the wires. This strong sensitivity to wire-bending also indicates that if random bends are present in the fabrication, this may introduce rather strong quenched disorder that will locally favor specific current patterns.

4.5 Summary

We summarize the degeneracy-lifting effects in the rough phase diagram shown in Fig. 7. For the parameters of the recent KT experiment [6] with straight wires, the non-zero wire width effect is dominant near the KT transitions and causes the system to order into the

$q = 0$ (---) phase. However, as we discuss above, bending the wires a little can counteract this effect and the amount of bending can be adjusted to stabilize any of the possible superconducting ordered phases.

This phase diagram (Fig. 7) is quite rough, showing just the simplest estimates of the locations of the phase boundaries. Certainly the sharp corners shown in the boundaries of the $q = 0$ and $\sqrt{3} \times \sqrt{3}$ phases are unrealistic; the true phase boundaries should be much smoother. Also, one should differentiate between the effects that lift the degeneracy of single triangles and those that produce interactions between triangles. Thus there should be at least two axes of degeneracy-lifting strengths. We leave a more careful exploration of the statistical mechanics of this interesting system for future researchers.

Another concern that we consider in the following section is the kinetics of this system. In order for this system to equilibrate, vortices must be able to move across the wire segments, producing phase slip and changing the current pattern. At too low temperature, these processes do not happen on laboratory time scales, and the system is frozen into a particular nonequilibrium current pattern. Thus for our novel ψ^3 superconducting phase to be realized in the laboratory, its KT transition temperature must be above the freezing temperature where the system stops being able to equilibrate.

5 Barriers to Vortex Motion

In the novel ψ^3 superconducting phase, the kagome-grid superconductor is not frozen into any one particular current pattern. One thing that could cause a selection of one pattern is a strong enough lifting of the degeneracy of the current patterns. Let us now assume that the net degeneracy-lifting effect is small enough that the equilibrium ordered phase is the ψ^3 phase. However, to realize this phase experimentally (or in a simulation), the system has to be able to equilibrate, which in this case means to be able to fluctuate among the many degenerate current patterns. The process by which the current pattern is changed is that of phase-slip or vortex motion. Here we will describe the vortices of the ψ^3 phase and estimate the barriers for their creation and motion in the vicinity of this phase's KT transition temperature. We find that the barrier for creation of a vortex pair is roughly $16k_B T$, which certainly slows down the dynamics considerably, and makes proper equilibration quite a challenge for a simulation study, but on the much larger time scales of experiment this barrier will not stop equilibration.

The vortices of ψ^3 that unbind at the KT transition of our novel phase are $1/3$ -vortices of ψ . The motion of these vortices also causes rearrangement of the current pattern. What do such fractional vortices look like? To make a pair of them, take a minimum-energy current pattern (for example, Fig. 2 (d)) and move a conventional superconducting vortex from a (+) triangle to an adjacent (−) triangle through phase slips across the wires or at the intervening junction, as shown in Fig. 8. This is equivalent to switching the circulations of these two adjacent triangles. The gauge-invariant phase gradients $\nabla_g \phi$ around the wire grids are rearranged such that the sum of $\nabla_g \phi$ around each triangle remains $\pm\pi$ and ψ is

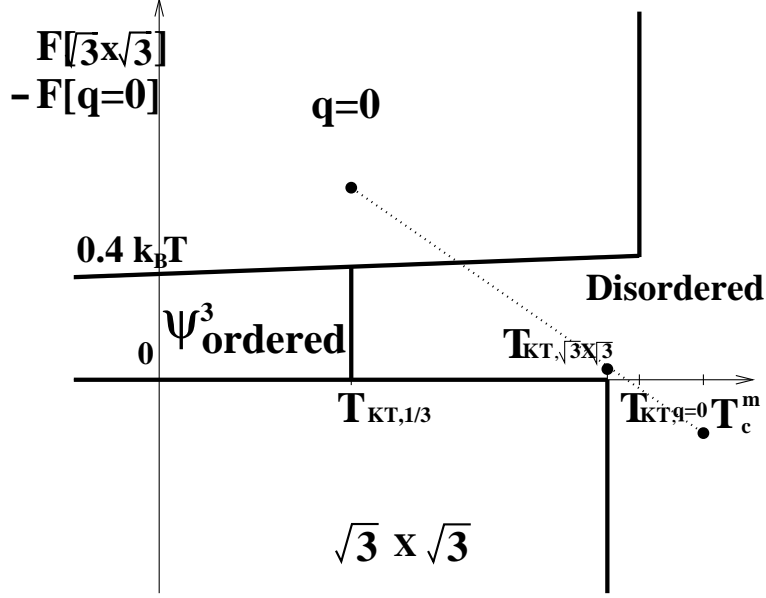


Figure 7: Rough phase diagram of the kagome superconducting wire network at $f = 1/2$. The horizontal axis is the temperature. We show only the narrow temperature range close to the mean field transition temperature T_c^m , where the Kosterlitz-Thouless transitions are. The vertical axis is the energy difference per unit cell between the $\sqrt{3} \times \sqrt{3}$ and the $q = 0$ patterns. The boundaries of the three superconducting phases are shown bold. The dotted line shows the path taken in this phase diagram for the experimental parameters that we consider (Appendix A). This system orders into a conventional superconducting phase with a $q = 0$ current pattern. As we discuss, the other phases can each be stabilized by bending the wire segments by a suitably chosen amount.

single-valued. This new current pattern is *not* one of the minimum-energy patterns. This rearrangement creates a pair of $\pm 1/3$ -vortices (see Fig. 8) of the ψ^3 phase. To see these $1/3$ -vortices we use the hexagonal unit cells shown dashed in Fig. 8, whose corners are at the centers of the elementary triangles of the kagome grid. The fractional vortices are different from ordinary vortices in the sense that the gauge-invariant vorticity $\oint(\nabla\phi - A)$ in a hexagonal unit cell may be an integer multiple of $2\pi/3$ instead of the usual 2π . Consider the $+1/3$ -vortex in Fig. 8. Since each triangle is shared by three hexagonal unit cells, we assume that each triangle contributes a third of its gauge-invariant vorticity of $\pm\pi$ to each of the three unit cells that overlap it. For the unit cell containing our $+1/3$ -vortex, there are four adjacent (+) triangles and two (−) triangles, and the gauge-invariant vorticity in the elementary hexagon is zero. Thus the net gauge-invariant vorticity in this hexagonal unit cell marked $+1/3$ is $+2\pi/3$. With this definition of the vorticity in a hexagonal unit cell, all minimum-energy current patterns are vortex-free, as should be the case for the ground state of an ordered phase. Once fractional vortices are present, they can also be moved by essentially the same process that creates the pair. For example, by switching the circulations of the two triangles which are indicated by the arrows in Fig. 8 we can move the $+1/3$ vortex to another location. This illustrates how a fractional vortex can move and how it rearranges the current pattern as it moves.

To estimate numerically the energy barriers to creating and moving $1/3$ -vortices, we need to find continuous paths in configuration space for these processes. We do this using the GL thin-wire limit free energy (3) on small systems with periodic boundary conditions, and discretized with a finite number of numerical grid points along each wire segment. [11] A continuous path from a given local minimum of the energy to a phase-slip event can be obtained by constraining the magnitude of the order parameter at the location of the phase slip and relaxing all the other degrees of freedom to minimize the energy with this constraint. Then the magnitude of the order parameter at the constrained point is decreased to zero and we follow the energy during this process. To find a path between two local minima that are simply separated by one phase-slip event, we approach from each minimum, thus making the connection. For the experimental parameters we use (Appendix A), and at the KT temperature of the ψ^3 phase, we find that the lowest saddle point for the fractional-vortex motion and pair creation processes is a phase-slip event occurring at or very near a junction. Thus it is the order parameter magnitude at that junction that we suppress to find the saddle point.

Extrapolating our numerical results to the continuum limit, we find that at the KT transition of the ψ^3 phase, the barrier for pair creation is about $16k_B T$, and the barrier for motion of the $1/3$ -vortices is about $7k_B T$. This implies that the probability of creating a $1/3$ -vortex pair is roughly $e^{-16} \cong 10^{-7}$ per unit cell per microscopic time scale. Although this is a small number, the size and time scales of the laboratory experiments are large enough that this process will not be frozen out at $T_{KT,1/3}$, and the system can equilibrate into the novel ψ^3 phase. For simulation studies, however, this small number means equilibration will be quite slow using standard simple algorithms [15]. This suggests

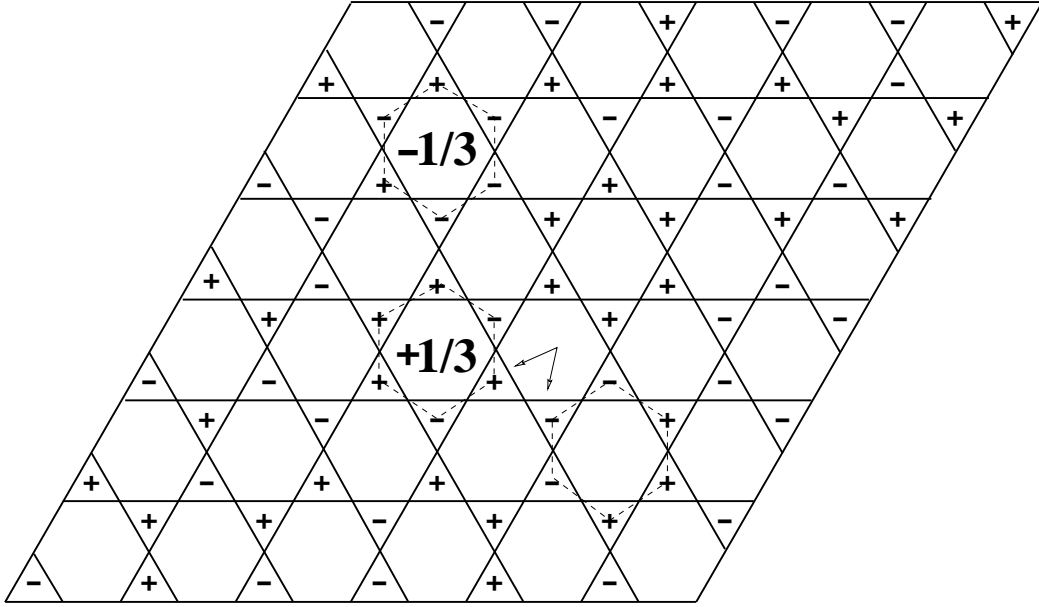


Figure 8: A pair of $\pm 1/3$ -vortices generated from a minimum-energy current pattern (Fig. 2 (d)) through phase-slip processes across the wires. The dotted lines represent hexagonal unit cells where $\pm 1/3$ vortices are defined. As one example of vortex motion, the $+1/3$ vortex can move to the empty hexagonal unit cell outlined by a dotted line through phase slips across the wires indicated by the arrows.

that simulation studies of this system should use special biased sampling moves of some sort that will enhance the rate of these phase-slip processes.

6 Conclusion

We have examined which superconducting state is stable among the $q = 0$, $\sqrt{3} \times \sqrt{3}$, and novel ψ^3 ordered phases at the Kosterlitz-Thouless (KT) transition in the kagome-lattice superconducting wire network at transverse magnetic field $f = 1/2$. We estimated the helicity moduli of the $q = 0$ and $\sqrt{3} \times \sqrt{3}$ patterns within the (straight) thin-wire GL theory without thermal fluctuations. In the GL regime, different minimum-energy current patterns have different helicity moduli because of the coupling between order parameter magnitude and phase distortions. The helicity modulus of the $\sqrt{3} \times \sqrt{3}$ pattern is lower than that of the $q = 0$ pattern. We use the helicity moduli to determine the KT transition temperatures for the ψ ordered phases and the novel ψ^3 phase. At these KT temperatures we estimated the single-triangle degeneracy-lifting effects (non-zero wire width and a possible bending of the wires) and the interactions between adjacent triangles (inductive coupling between adjacent supercurrents, order-by-disorder caused by thermal fluctuations, and also a non-zero wire-width contribution). For the experimental parameters (Appendix A), the system with straight wires becomes ordered into a conventional superconducting phase with the $q = 0$ (—) current pattern due to the dominant finite wire width effect. But this finite wire width effect can be adjusted experimentally by fabricating the wires narrower (with a fixed lattice constant a) or, perhaps more easily, such that they are bent away from the straight line between junctions by an amount that restores the degeneracy. Both ways can reduce the finite wire width effect so that the system can be stabilized into the novel ψ^3 superconducting phase. The energy barriers for creating and moving $1/3$ -vortices are low enough that the experimental system can equilibrate at and even a little below this KT transition.

Appendix

A Experimental Parameters

For comparison to our analysis, we use the following values of the parameters, as in the recent experiment [6] on an aluminum kagome-lattice wire network: The number of unit cells is of order 10^5 . The distance between junctions (a) is 20000\AA . The width (w) and thickness (d) of the wires are 2000\AA and 500\AA , respectively. The zero-field transition temperature T_c^m is $1.183K$. The amplitude of the mean-field coherence length in zero field scaled by a , (ξ_0/a) , can be estimated experimentally by comparing the measured phase boundary $T_c^m(f)$ with the mean-field phase boundary obtained theoretically by Lin and Nori [8]. Experimentally, it is found that the shape of the $T_c^m(f)$ curve agrees well with

the theory when a criterion of some value between $1/20$ and $1/30$ of the normal state resistance is used to define $T_c^m(f)$. This correspondence yields $(\tilde{\xi}_0/a) \cong 0.054$. From the nonlinear current-voltage characteristics, the KT temperature at $f = 1/2$ is measured to be: $T_c^m(f = 1/2) - T_{KT}(f = 1/2) \cong 7.6mK$.

Since the temperatures that we are interested in are all near the zero-field transition temperature T_c^m , we use the following approximate expressions [16] for the thermodynamic critical field $H_c(t)$, the coherence length $\xi(t)$, and the penetration depth $\lambda(t)$, where t is the reduced temperature T/T_c^m .

$$\begin{aligned} H_c(t) &\cong 1.73H_c(0)(1-t) , \\ \lambda(t) &\cong \frac{\lambda_L(0)}{\sqrt{2(1-t)}} \left(\frac{\xi^{(cl)}(0)}{1.33l} \right)^{1/2} , \\ \xi(t) &\approx \tilde{\xi}_0(1-t)^{-1/2} \cong 0.855 \left(\frac{\xi^{(cl)}(0)l}{1-t} \right)^{1/2} , \end{aligned}$$

where for aluminum samples [17][18],

$$H_c(0) \cong 100Oe, \quad \xi^{(cl)}(0) \cong 16000\text{\AA}, \quad \lambda_L(0) \cong 160\text{\AA}, \quad l \cong 100\text{\AA}.$$

Our estimate of the mean free path l comes from the value $\tilde{\xi}_0 \cong 0.054a$. The expressions for the coherence length and penetration depth are for the dirty limit, while $\xi^{(cl)}(0)$ is the low-temperature coherence length in the clean limit. The dirty limit applies to the samples and temperatures we consider. This sample falls in the type-II regime

$$\kappa|_{\text{dirty limit}} \cong 0.715 \frac{\lambda_L(0)}{l}, \quad (39)$$

although clean aluminum is a type-I superconductor.

References

- [1] A. B. Harris, C. Kallin and A. J. Berlinsky, Phys. Rev. B **45**, 2899 (1992).
- [2] R. J. Baxter, J.Math.Phys. **11**, 784 (1970).
- [3] David A. Huse and Andrew D. Rutenberg, Phys. Rev. B **45**, 7536 (1992).
- [4] M. S. Rzchowski, Phys. Rev. B **55**, 11745 (1997).
- [5] J. M. Kosterlitz and D. Thouless, J. Phys. C **6**, 1181 (1973); J. M. Kosterlitz, J. Phys. C **7**, 1046 (1974).
- [6] Yi Xiao and Paul M. Chaikin, private communication. We use their unpublished data of the aluminum kagome-lattice wire network. The detailed experimental parameters are shown in Appendix.

- [7] M. J. Higgins, Yi Xiao, S. Bhattacharya, P. M. Chaikin, S. Sethuraman, R. Bojko, and D. Spencer, Phys. Rev. B. **61** R894 (2000).
- [8] Qin Niu and Franco Nori, Phys. Rev. B **39**, 2134 (1989); Yeong-Lieh Lin and Franco Nori, Phys. Rev. B **50**, 15953 (1994).
- [9] P. M. Chaikin and T. C. Lubensky, *Principles of condensed matter physics*, (Cambridge University Press, New York, 1995).
- [10] J. D. Jackson, *Classical Electrodynamics*, (John Wiley & Sons, New York, 1975).
- [11] Kyungwha Park, Ph.D. Thesis, Princeton U. Physics Dept. (2000).
- [12] J. Villain, R. Bidaux, J. P. Carton, and R. Conte, J. Phys. (Paris) **41**, 1263 (1980).
- [13] Christopher L. Henley, Phys. Rev. Lett. **62**, 2056 (1989).
- [14] J. T. Chalker, P. C. W. Holdsworth, and E. F. Shender, Phys. Rev. Lett. **68**, 855 (1992).
- [15] K. Binder and D. W. Heermann, *Monte Carlo Simulation in Statistical Physics*, (Springer-Verlag, Berlin Heidelberg, 1997).
- [16] Michael Tinkham, *Introduction to Superconductivity* (McGraw-Hill, New York, 1996).
- [17] B. W. Roberts, 9g in *American Institute of Physics Handbook*, ed. by Dwight E. Gray, (McGraw-Hill, New York, 1972).
- [18] Charles Kittel, *Introduction to Solid State Physics*, (John Wiley & Sons, New York, 1986).